Defence Science Journal, Vol. 72, No. 3, May 2022, pp. 309-319, DOI : 10.14429/dsj.72.3.16647

Effect of Explosive Shapes (in Sand Buried Condition) on the Failure of a Circular Clamped Plate of Protective Vehicle

Pankaj K. Choudha,[#,*] A. Kumaraswamy[$] and V. Venkateswara Rao[#]

[#]*DRDO - Armament Research & Development Establishment, Pashan, Pune - 411 021, India*

[$]*Dept of Mechanical Engineering, Defence Institute of Advanced Technology, Girinagar, Pune – 411 025, India*

[*]*E-mail: pkchoudha@gmail.com*

ABSTRACT

Protective vehicles like armoured personnel carriers (APCs) require assessment of failure of structural elements subjected to impulsive load resulting from explosive blast under sand buried conditions. The explosive shape and location of detonation affect the failure in near field region. In the present study, a circular clamped Rolled Homogenous Armour (RHA) steel plate has been modelled using JC strength & damage model and explosive using JWL equation. Initially, the reflected pressure and specific impulse for a fixed quantity of explosive (3.75 kg) of various shapes i.e. sphere, hemisphere, cylinders with Length to Diameter (L/D) ratio varying from 0.1 to 1 were studied for sand buried at a standoff distance of 118.1 mm. Further, studies were extended for cylindrical charges of ϕ 213.77 mm with conical 120°-150° and hemispherical cavities with radius of R1.2-R1.8. It was observed that, reflected pressure and specific impulse is much higher for hemispherical cavity of R1.2. The permanent deformation obtained using non-dimensional impulse is valid for explosives without cavities. However, the cavity charges produce failure of plate in the central region of the charge. The critical impulse emerges as an important parameter for assessing failure due to cavity charges. In addition, the scale down experiment is conducted to validate the effectiveness of cavity charges. It can be concluded that cavity charge with hemispherical radius of R1.2 can provide highest damage to RHA plates in close standoff distance.

Keywords: Armour steel; Explosive shape; Conical cavity charge; Hemispherical cavity charge; Detonation point; Large inelastic deformation

NOMENCLATURE

ρ_e	: Explosive density
a, b	: JWL constant
R_1, R_2, ω	: JWL constant
D_e	: Detonation velocity
Q_e	: Specific internal energy
Pcj	: CJ detonation pressure
L	: Length of explosive charge
D	: Diameter of explosive charge
R	: Radius of explosive charge
P	: Pressure
ν	: Poisson's ratio
q	: Specific heat
ρ	: Density
E	: Young modulus
A	: Yield stress
B	: Hardening constant
n	: Hardening exponent
C	: Strain rate constant
m	: Thermal softening exponent
T_m	: Melting temperature
$\dot{\varepsilon}_0'$	: Reference strain rate
σ_m	: Mean stress
σ_{eq}	: Equivalent Stress
D_1-D_5	: JC damage constants
ε_f	: Failure strain
ρ_a	: Air density
E_a	: Internal energy of air
γ	: Ratio of specific heats
T	: Temperature
ρ_s	: Density of sand
σ_y	: Yield Stress
c	: Sound velocity of sand
G_s	: Shear modulus of sand
σ_y	: Yield stress for sand
t	: Plate thickness
R_p	: Radius of plate
S	: Standoff between explosive and plate
δ_d	: Dynamic deformation per unit plate thickness
δ_p	: Permanent deflection per unit plate thickness
ε_{fr}	: Fracture strain

Received : 12 January 2021, Revised : 06 December 2021
Accepted : 14 March 2022, Online published : 01 July 2022

$(I_0)_{cr}$: Critical impulse

$\varnothing_{cs}$: Non-dimensional impulse

1. INTRODUCTION

Anti-tank mines extensively used for defence during the war are a serious threat to military vehicles such as trucks, APCs, Main Battle Tanks (MBTs), and mine clearing systems. The damaging methods employed for these targets are a blast and hollow charge principle while damage of the vehicles in case of blast mines is credited to the transfer of shock waves. Held divided the blast load mainly into two categories i.e. close field and global effects. Close field-effect deform the belly of tanks whereas global effects accelerate the total vehicle with enormous force leading to damage[1]. Björn, *et al.* have assessed the damage due to buried land mines in the near-field region. The extent of the near-field region is generally considered in the range 0-20 times the radius of explosive charge[2]. Trinitrotoluene (TNT) has been used as the explosive for the majority of the experimental studies. In addition, the blast parameters of other explosives can be converted to TNT equivalence for near field with variable equivalent factors and far-field blast region with constant equivalent factors[3]. Peak pressures at near and larger scale distances differ due to the shape of explosives i.e. spherical, cylindrical, and planer[4]. To evaluate the near field damage effects, detonation location of explosives is an important parameter for ammunition designers.

The cylindrical shapes with different L/D ratio will produce different near filed effects as reported by various researchers. Knock, *et al.* have studied cylindrical charge with various aspect ratios in free air blast parameters' prediction in axial and radial directions[5-7]. Wu, *et al.* carried out a study of cylindrical charge with length (L) to diameter (D) ratio of 0.5-2 for reflected peak overpressures with a minimum scale distance of 1.5 m/kg$^{1/3}$, with the detonation point at the geometric center and end of explosive. It was concluded that a cylindrical charge along the axis produces a much higher reflected pressure and impulse on a target, as compared to a spherical charge in the near field region. The smaller L/D ratio of the cylindrical charge helps in focusing more energy in the axial direction[8-9].

The near filed blast produced by explosive will create impulsive loading on structural elements likes beams and plates. The mild steel and Rolled Homogeneous Armour (RHA) steel are the most common materials used for the evaluation of lethal effects in many defence applications[10]. Deformation and failure are important areas of investigation for all structures due to impulsive loading. A significant amount of experimental and simulation work has been carried out to understand the deformation with the variation of explosive quantities, standoff distances using pendulum-based impulse measurement techniques.[11-16]

Reflection and enhancement of impulsive loads produced by explosive blast due to presence of various mediums are studied by many researchers. Gault, *et al.,* have studied the evolution of the shock wave parameters experimentally to predict the origin of the first three reflected peaks in closed rooms[17]. The effect of confinement on reflected blast parameters is reported by Ambrosini *et al.*[18] Peles *et al.* studied the cylindrical charge for influencing armour damage with respect to charge geometry, standoff distances, charge buried conditions, and soil properties[19]. Heider and Klomfass discussed that increasing thickness of the sand cover decreases the peak values directly above the mine and still increases cumulated momentum within a certain sand layer thickness[20]. Hoyos *et al.* reported the dependence of compaction and moisture content of sand in the impulse transfer to a rigid object[21]. Clarke *et al.* discussed the effect of air voids and moisture content on impulse and deformation of the plate with five different grades of soils. An empirical relationship for the estimation of impulse was proposed based on a percentage of moisture content and bulk densities. Very low deflections were observed in clay experiments in spite of having the highest total impulse due to distribution over plate[22]. Significant increase in the impulse recorded in experiments due to focussed blast by the surrounding sand[23]. The highest transfer of impulse was observed for buried charges located just under the surface. Therefore, it is the ideal representation of landmines for laboratory-scale experiments and studies[24]. Scaling of the deformation histories is reported for clamped circular plates subjected to loading by buried charges[25].

The correct impulsive load estimation plays an important role in study of deformation and damage behaviours of plates. It was found that the predicted final transverse displacements for the above pulses loads are highly dependent on the pulse shape[26]. Chung, *et al.* reviewed the deformation of circular and rectangular steel plates using non-dimensional impulse[14]. Various analytic models for deflection of the plate due to blast loads were compared with experimental data by Gharababaei *et al*[27]. Three stages of dynamic response, i.e. dishing, discing, petalling and permanent shape of the plate is strongly dependent on the spatial distribution of pressure loading. In addition, more localised deformation at the plate center was observed for the smaller loaded area and more distributed load led to tearing failure at the clamped boundary[28]. Walters brought out that the Munroe effect, i.e., hollow cavity charge can enhance the damage effect[29]. The author had earlier reported the damage of the RHA plate with cavity charge[30]. Simulation techniques are well reported for studying the deformation and failure due to explosive blast loading using 2-D and 3-D analysis by available hydrocodes i.e. LS-Dyna, AUTODYN[31-36].

A comprehensive literature review revealed that these mines have explosive charges of cylindrical shapes with their weights in the range of 3-12 kg. In addition, many studies related to the blast of buried charges were carried out with an L/D ratio of 0.25-0.3 only. However, any investigator has not reported the change in the shape of explosive and detonation point location on deformation behavior yet.

In order to address the gaps highlighted above albeit partially, in the present study, a series of simulations are carried out using 2D axisymmetric analysis. Most common explosive shapes employed in land mines like spherical, hemispherical, cylindrical, and cylindrical with conical and hemispherical cavities are considered. The effects on reflected pressure, specific impulse, and total impulse are studied at very close standoff distances with these explosive charges. Additionally, the cylindrical shape of L/D=0.3 is studied at much closer

standoff distances. The failure of RHA plates are studied to bring out the potential deformation and damage capability of a fixed quantity of explosives with different shapes in sand buried conditions. The damage using the non-dimensional and critical impulse is compared with simulations results. Further, scale-down experiments are conducted to validate the simulation results.

2. NUMERICAL SIMULATION

AUTODYN hydrocode for numerical simulations allows users to deal with the dynamic response of structures subjected to blast loads using Lagrangian, Eulerian, and Smoothed Particle Hydrodynamics (SPH) methods for modeling fluid-structure interaction. These methods are used in combination for solving most of the blast-structure interaction problems. Specific impulse variations as a function of distance from the blast center are analysed first to gain insights into the effect of interaction between blast wave and plate in terms of reflected pressure and specific impulse distribution.

2.1 Simulation Model

Neuberger, *et al.* have carried out experiments with 3.75 kg of TNT explosive for determining the deformation of Rolled homogenous armour (RHA) steel[38]. The RHA plate of 1 m and 20 mm thickness is mounted on a heavy rigid rectangular stand of approximately 750 x 750 mm^2 with a central cut out of radius of 500 mm. Two backplates of 50 mm and 100 mm are used for holding the main plate during the experiment. TNT is buried from the center of a charge in the sand at a standoff distance of 200 mm from the plate[37-38].

To finalise the parameters of the simulation, 2-D axis-symmetric analysis with symmetry about the X-axis is finalised. Initially, the plate with two backplates is modeled using Lagrange elements. The movements of the plates are restricted in both X and Y directions as per experimental setups. The contact elements are applied between the main plate and two backplates. To simulate the blast effect, the Euler domain of 750 × 750 mm^2 sizes is defined with sand up to 581.9 mm and air between 581.9 to 750 mm. The TNT (163.81 mm) is defined in the Euler domain and the detonation is defined at the center of the explosive. Flow out boundary conditions

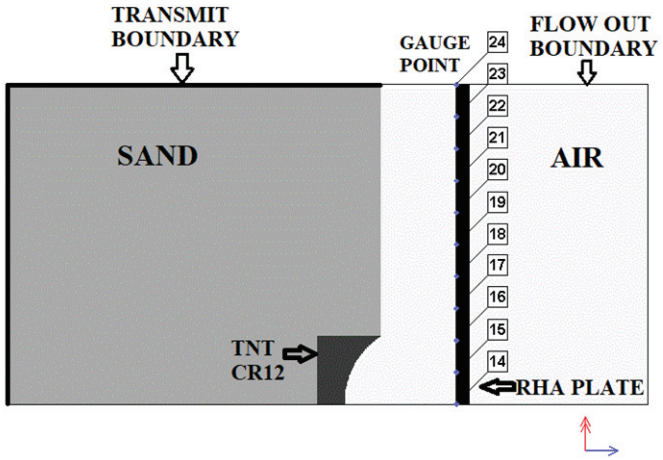

Figure 1. 2-D axis symmetric numerical models for RHA deformation of the plate.

are applied on the air domain and transmitting boundaries are defined for sand. 11 gauges were used in the simulation to monitor the deflection of the plate at every 50 mm distance from the center of the plate. These gauges record the deflection time history of the plate.

After completing the simulation, the study of Neuberger *et al.* experimental setup, a simplified simulation model as shown in Fig. 1 was used to study the shape effect on the deformation of RHA plate in sand buried condition. The TNT charge shape of the cylinder with the hemispherical cavity of 1.2R is shown in Figure 1. The transmitting boundary condition on sand allows the pressure wave to pass through the boundary and does not reflect them and simulate the infinite sand media or ground. The flow-out boundary condition on the airside allows the air to flow out of the domain and represent the free air expansion with reflection from the boundary.

2.2 Material Model and Properties

Three materials involved in the simulation process namely explosive, RHA steel, and sand are important. The explosion is modeled using the JWL equation of state. The detonation is initiated at the detonation point and the detonation front progresses spherically and reaches the un-reacted explosive material. The unreacted explosive material is converted into

Table 1. Material properties of TNT and air[32]

JWL material parameters for TNT			Properties of air		
Parameters	**Value**	**Unit**	**Parameters**	**Value**	**Unit**
ρ_e	1.63 ×10^3	kg/m^3	ρ_a	1.225 ×10^3	kg/m^3
a	3.7377×10^{11}	Pa	γ	1.4	
b	3.7471×10^{10}	Pa	T	283	°K
R_1	4.15		q	717.3	J/kg °K
R_2	0.90		E_a	2.068 ×10^5	kJ/m^3
ω	0.35				
V_d	6930	m/s			
Q_e	6.00×10^9	kJ/m^3			
P_{cj}	2.1×10^{10}	Pa			

gaseous products and releases the energy to the associated element. JWL equation of state (EOS) is given in equation (1). JWL parameters of TNT explosives are given in Table 1.

$$P = a\left(1-\frac{\omega\eta}{R_1}\right)e^{-\frac{R_1}{\eta}} + b\left(1-\frac{\omega\eta}{R_2}\right)e^{-\frac{R_2}{\eta}} + \omega\rho Q_e ;$$

$$\text{Where, } \eta = \frac{\rho}{\rho_e} \quad (1)$$

The air is modeled using the 'ideal gas' equation of state given in Eqn. (2). The properties of air are given in Table 1. To define the atmospheric pressure of 101.4 KPa, the internal energy is used.

$$P = (\gamma - 1)\frac{\rho E_a}{\rho_a} \quad (2)$$

The Johnson and Cook (JC) strength material model is well known for including the strain rate effect, work hardening effect, and thermal softening effects. The JC strength model is defined by Eqn. (3). Further, the JC damage model can be utilised to make the failure strain sensitive to stress triaxiality, temperature, strain rate, and strain path[39]. This model assumes that the damage accumulates in the material element during plastic straining which accelerates immediately when the damage reaches a critical value. The JC damage model is defined by equation (4). The parameters for a RHA material are given in Table 2.

$$\sigma = \left(A + B\varepsilon^n\right)\left(1 + C\log\dot{\varepsilon}^*\right)\left(\frac{T - T_r}{T_m - T_r}\right)^m ;$$

$$\text{where } \dot{\varepsilon}^t = \frac{\dot{\varepsilon}^t}{\dot{\varepsilon}_0^t} \quad (3)$$

$$\varepsilon_f = \left[D_1 + D_2\exp\left(D_3\frac{\sigma_m}{\sigma_{eq}}\right)\right]\left[1 + D_4\ln\left(\dot{\varepsilon}\right)\right]\left[1 + D_5\left(\frac{T - T_r}{T_m - T_r}\right)\right] \quad (4)$$

Table 2. JC strength & damage model parameters for RHA Steel[37-39]

Strength model parameters			Damage model parameters		
Parameters	**Value**	**Unit**	**Parameters**	**Value**	**Unit**
ρ	7.85×10^{3}	kg/m^3	D_1	5.00×10^{-2}	
ν	0.33		D_2	8.00×10^{-1}	
E	2.03×10^{11}	Pa	D_3	-4.40×10^{-2}	
A	9.5×10^{08}	Pa	D_4	-4.6×10^{-2}	
n	0.26		D_5	0	
B	5.600×1008	Pa	$\dot{\varepsilon}_0^t$	1	
C	1.40×10^{-2}	s^{-1}			
m	1				
q	452	J/kg °K			
T_m	1783	°K			
$\dot{\varepsilon}_0^t$	1×10^{-4}				

A study for buried charges was carried out by Pickering *et al.* considering the Laine and Sandvik sand model[24]. Laine and Sandvik presented a sand model consisting of MO Granular strength model defined by sand density, shear modulus, yield stress, and compaction pressure with a linear unloading method for the EOS. The compaction EOS is dependent on the sand density, compaction pressure, and wave speed. The yield surface for a Granular strength model is dependent on both density and pressure. This model is pressure dependant only therefore zero values for σ_y in column 6 of Table 3 are assumed. The parameters defining the curves are given in Table 3.

Table 3. Data points for the curves that define the sand material model[24]

ρ [kg/m^3]	P ×10^6 [Pa]	ρ [kg/m^3]	C [m/s]	G [Pa]	σ_y [Pa]	P ×10^6 [Pa]	σ_y [Pa]
1674	0	1674	265	0.08	0	0	0
1740	4.6	1746	852	0.87	0	34	4.2
1874	15	2086	1722	4.03	0	34.9	44.7
1997	29.2	2147	1876	4.91	0	101.3	124
2144	59.2	2300	2265	7.77	0	184.7	260
2250	98.1	2572	2956	14.80	0	500	260
2380	179.4	2598	3112	16.57	0		
2485	289.4	2635	4600	36.72	0		
2585	450.2	2641	4634	37.35	0		
2671	650.7	2800	4634	37.35	0		

2.3 Validation of Numerical Models

To begin with, a simulation model is validated by using the coupled Lagrange and Euler technique. The convergence parameter was checked for mid-point deflection of the plate. Initially, the size of the Euler element of 3 mm and the Lagrange element of 5 × 2. 5 mm were considered for air and plate receptively. The detonation point D1 was used for validating the model. The experimental deflection reported by Neuberger, *et al.* was 54.0 mm[37].The deflection of 48.76 mm was observed against 54.0 mm with error of -9.70%. To improve the results further, the Euler element size was reduced to 1 mm in the vicinity of 100 mm from the X-axis and biased to increase to 1.5 mm at the end of the Euler domain. It has been observed that Case-II with the plate element of 5×2.5 mm with Euler elements of 1-1.5 mm produces the best results. The deflection obtained is 52.46 with only -2.85% error for air blast simulation. The air was replaced with sand as shown in Fig. 1 and transmitted boundary conditions was applied to the sand boundary. The deflection of 122.25 mm was obtained in the simulation against experimental deflection of 120 mm reported by Neuberger, *et al.*[38] with +1.87% error. Therefore, all the further studies were carried out with these parameters.

3. EFFECT OF CHARGE SHAPES ON IMPULSE AND PRESSURE

Initially, in understanding the effect of explosive shapes

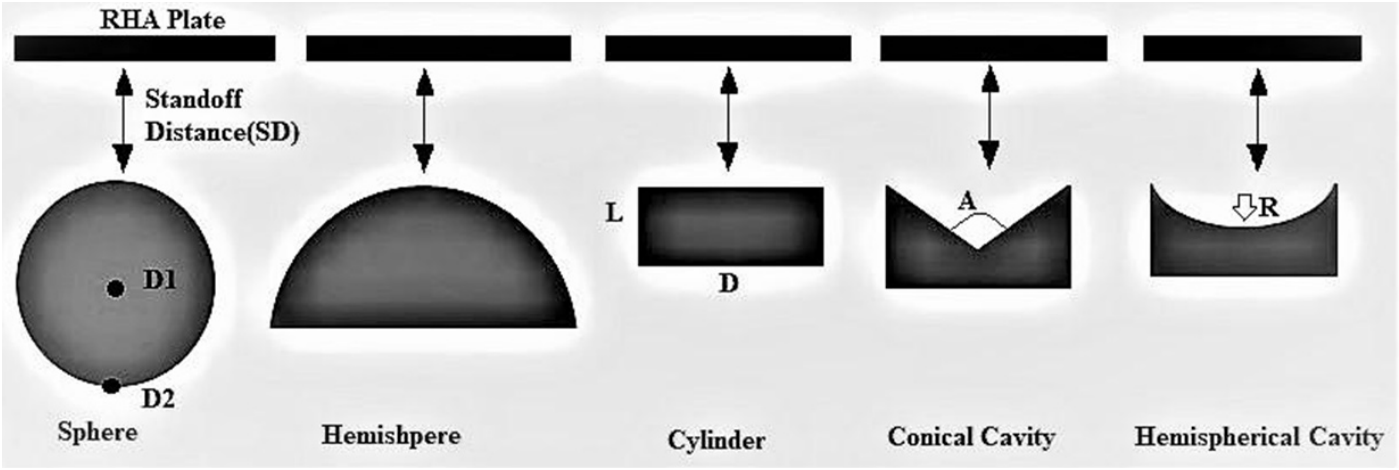

Figure 2. Geometry of explosives considered for simulation

Table 4. Dimensions of various geometry of charge

Charge shape	Charge dimension		Charge shape	Charge dimension	
	ϕ	L		ϕ	L
Sphere (S)	163.8	-	Cone Cavity 120° (C120)	213.8	84.7
Hemisphere (HS)	206.4	-	Cone Cavity 150° (C150)	213.8	73.7
Cylinder (L/D=1) (C1)	143.1	143.1	HS Cavity of R1.8 (CR18)	213.8	100.5
Cylinder (L/D=0.6) (C06)	169.7	101.8	HS Cavity of R1.5 (CR15)	213.8	81.7
Cylinder (L/D=0.3)(C03)	213.8	64.1	HS Cavity of R1.2 (CR12)	213.8	74.7
Disc (L/D=0.1) (C01)	308.3	30.8	-	-	-

and detonation points, is to study the distribution of blast pressures and specific impulses with space and time on a rigid plate kept at a fixed standoff distance of 118.1 mm from the charge surface. The explosive of 3.75 kg in spherical, hemispherical, and cylindrical shapes having L/D 1, 0.6, 0.3, and 0.1 are studied. In addition, the cylindrical charge of ϕ213.8 mm having a conical cavity of 120º-150º and hemispherical cavity of radius 1.2R, 1.5R, and 1.8R of charge are also studied. Cylindrical charges with C03 were considered for deciding the hemispherical and conical cavities based on the practical application of land mines. Therefore, the charge diameter of ϕ213.8 mm was fixed and the length of the charge was fixed based on the mass of the explosive charge. The initiation point of the explosive charge is considered to be either at the far end to plate (D2) or at the geometric center (D1) as shown in Fig. 2. The results with the suffix of 'E' indicate the end initiation. The dimensions of the charges are given in Table 4.

To study the pressure and specific impulse distribution with time and space, a rigid boundary model is considered. Initially, the detonation point D1 was used for validation, and later on D2 point was used. It was observed that the D2 point produces more deflection compared to the D1 point. Therefore, D2 was considered in all further analysis, which is discussed in the following paragraphs.

3.1 Total Impulse on Plate

The 2-D axis-symmetric model is used here for obtaining pressure histories from the rigid boundaries as shown in Fig. 1. The model is in the Euler domain. The rigid boundary is specified at the interface of the plate and air to obtain the reflected pressures at the defined gauge points. The rigid boundary simulation allows no transmission of material and thus acts as a perfect reflecting surface. Flow-out boundary conditions are applied at the other outer edges of the Euler mesh. Mehreganian *et al* have carried out experimental studies with the rectangular plate of 400×400 mm with the explosive PE4 weighing 40 g (ϕ25 mm × 12.72 mm) at a standoff distance of 25 mm from AMX 370T steel plate[40]. To validate the impulse calculation, this problem was simulated using the axis-symmetry rigid boundary model proposed by Bonorchis and Nurick[2] with a diameter of 225.7 mm. The material properties are taken from the same reference. Eleven gauge points at equidistance at 22.57 mm from the axis are placed and the specific impulse is recorded. These values were multiplied by the element area. The total estimated impulse was found to be 78.75 N-s as compared to the experimentally reported value of 80 N-s. This input is used to decide the number of gauges to be placed in the air on the boundary.

For the current study, an Euler domain of 1000 x 500 mm^2 is used. The charge center is placed at 500 mm from the origin. The rigid boundary is considered at 700 mm i.e. 200 mm from the charge center of the charge. The flow-out boundaries are defined at the start and the radially extreme positions of the domain. Figure 1 shows the sand buried charge condition. The RHA plate was replaced with a rigid boundary and then pressure

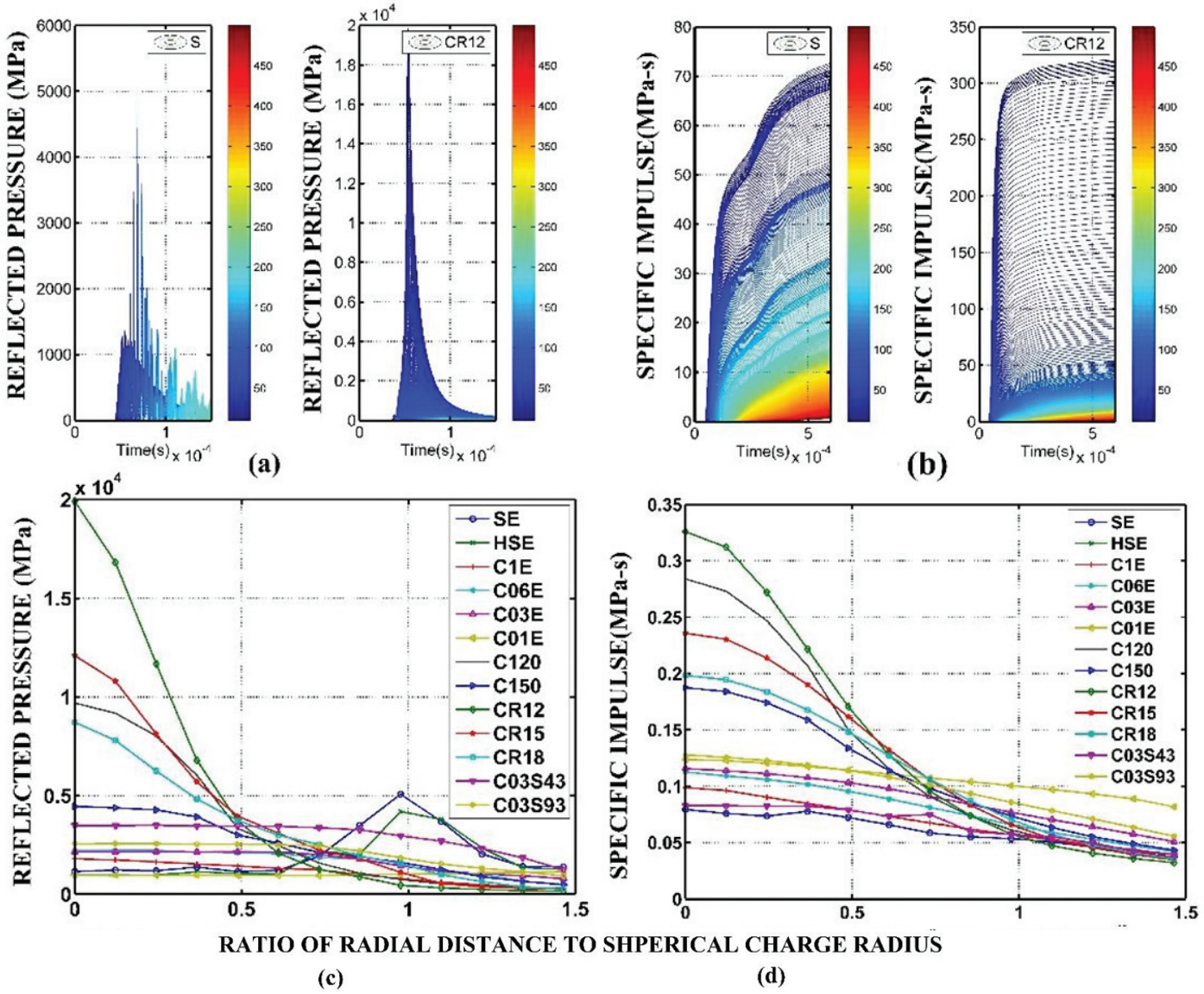

Figure 3. Pressure and specific impulse distribution for various shapes of explosives.

gauges are placed on the rigid boundary. 31 gauges are placed in the Euler domain at 700 mm to record the pressure data. 26 gauges at an equal distance of 10 mm are placed between 0 - 250 mm radial distance from the center of the plate. In addition, five more gauge points are placed at a 50 mm radial distance, between 250 - 500 mm. The results of these simulations are plotted in Fig. 3(a) for pressure distribution and Fig. 3(b) for specific impulse.

3.2 Effect of Explosive Shape

The reflected pressures and specific impulses for end initiation (D2) are studied for sand buried conditions. The pressure and impulse is plotted in Fig. 3(a) & Fig. 3(b) with respect to time and radial distance using the contour plot. The reflected pressure contour in Fig. 3(a) and specific impulse contour in Fig. 3(b) is plotted to show the distribution of pressure over the plate diameter. The pressure in case of spherical shape charge is distributed upto 250 mm radius of plate whereas the pressure is mostly concentrated in the 50 mm radius for explosive shape of CR12. The peak reflected pressure is observed to be 2202 MPa for cylindrical charges with C06E and C03E up to 80 mm radial distance from centre of the charge. However, it is only 973.93 MPa for C01E. The peak reflected pressure for SE and HSE cases are low i.e. 1150.6 MPa and 953.8 MPa respectively at the centre. The pressure increases to 5070 MPa and 4193.3 MPa at 80 mm radial distance from the centre. This is due to the diversion of high pressure gases radially out from the centre after interacting with the rigid boundary and also the direct air shock reaching in the region at the same time. In case of the buried hemispherical cavity charge CR12, the maximum pressure of 19922 MPa is observed which reduces to 2154.3 MPa at about 60 mm radial distance as shown in Fig. 3(c). CR15 produces less reflected pressure (12099 MPa) as compared to CR12.

The impulse of various buried charges are plotted in Fig. 3(d). The maximum impulse of 0.12347 MPa-s is observed in the case of disc charges having an L/D=0.1 (C01E). It is comparatively less for C03E i.e. 0.11566 MPa-s. The specific

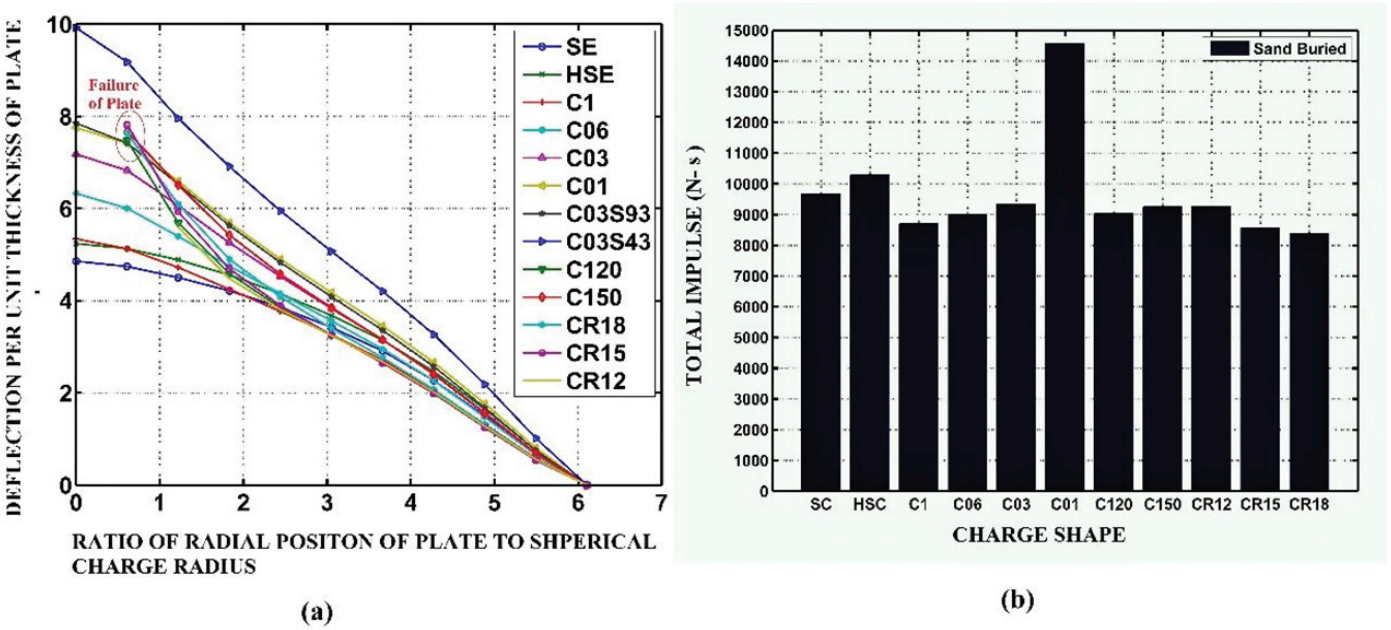

Figure 4. RHA plate deformation and total impulse on a plate for different shapes.

Table 5. Permanent deformation of charge geometry - Non-dimensional impulse and simulation

Charge	Impulse (N-s)	$\varnothing_{cs}$	δ_p	δ_{ps}	Difference
Sphere (S)	9678.4	11.591	5.247	4.572	-0.675
Hemisphere (HS)	10291	13.615	6.111	4.572	-1.539
Cylinder (L/D=1) (C1)	8703.4	9.942	4.543	5.110	0.566
Cylinder (L/D=0.6) (C06)	9024.5	10.956	4.976	6.092	1.115
Cylinder (L/D=0.3)(C03)	9346.3	12.587	5.672	6.961	1.289
Disc (L/D=0.1) (C01)	14582	25.201	11.058	7.557	-3.501
C03-SD43.1	13704	20.30	8.96	9.92	-0.95
C03-SD 68.1	12096	17.89	7.94	8.72	-0.78
C03-SD 93.1	10331	15.26	6.82	7.85	-1.04
C03-SD 108.1	9650	14.08	6.31	7.44	-1.12

impulse of the spherical buried charge is only 0.079371 MPa-s. In case of cavity charge, the specific impulse is much higher i.e., 0.33216 MPa-s for CR12. The impulse reduces to 0.099091 MPa-s at 60 mm radial distance. The results were compared for total impulse transferred to the rigid plate. It indicates that the total impulse is highest for the disc C01E shape i.e. 14582N-s, followed by HSE and SE shapes. The explosive disc C01E covers the larger area of plate with less thickness and therefore pressure is low. This shape causes the highest total impulse but does not lead to the failure of RHA. The total impulse in the case of cylindrical and cavity charges is not having the much difference as shown in Fig. 4(b).

Similar studies carried out by Peles, *et al.* reported the enhancement in deformation of the plate with cylindrical charge shape having larger diameters and shallowly buried conditions[19]. Also, in current studies, CR12 and conical cavity C120 charge shapes have shown enhancement of reflected pressure and specific impulse. Similar enhancement for conical and elliptical cavities using the SPH technique is reported by Liu *et al*[41]. The reason for enhancement in pressure and specific impulse is due to cavity in explosive charge. When the cavity is created in explosives, the detonation products converge to the central axis and move perpendicular to the original cavity surface and concentrate along the axis and forming a jet of very high kinetic energy gases. The shapes of conical and hemispherical cavities produce different densities, pressure, and velocity distribution of gas jets, which may be used in damaging the plates.

4. DEFORMATION OF RHA PLATE- DISCUSSION

4.1 Influence of Charge Shape

The simulations for deformation of the plate in sand buried conditions for all explosive shapes are carried out. The model used is shown in Fig. 1. Eleven gauge points at 50 mm distance are placed on the plate. Displacements of the plate

on these gauge points are recorded. The simulations are carried out in two stages. In the first stage, the interaction between gases in the Euler domain and the plate is carried out for 1.5 ms. In second stage, the simulation with deactivation of the Euler domain was run up to 7.5 ms. Dynamic deformation of the plate is observed. The permanent deformation was calculated by averaging the peaks of the oscillating deformation between 1.5-7.5 ms duration.

The dynamic deformation of all the charges shapes are plotted in Fig. 5(a). Cavity charges become more damaging and the failure occurred in all types of cavity charges as shown in Fig. 5(a). The deformation is observed as δ_d =7.752 for C01E and δ_d =7.178 for C03E. The failure of the RHA plate is observed at the center in each of the cavity charges. The failure in each case initiates at different instances, ranging from δ_d = 2.4207 to 4.6756. The charge CR12 has a larger failure radial distance, which is more than 50 mm. The maximum deformation of the plate is 7.8167 in the case of CR15. However, all the deformations are similar in nature. The dynamic deformation shape of plates with respect to shapes show that the impulse distribution will affect the shape of the deformation of the plate. The shape of spherical and hemispherical will produce the dome shape deformation whereas cylindrical shape charges will produce the double cone deformation. The inner cone has the larger deformation compared to the cone at the clamp side. Therefore, the failure was observed in the case of cavity charges.

4.2 Influence of Stand off Distances

To analyse the L/D=0.3 cylindrical charges, which can cause failure in shorter standoff distances have been evaluated in buried charge condition. The standoff distances (S) were reduced to 108.1, 93.1, 68.1 and 43.1 mm. The peak reflected pressure and impulse in the case of are shown in Fig. 5. It has been observed that reducing the standoff distance can increase the deformation, as shown in Fig. 5(a). However, no failure of the plate was observed even at the lowest standoff distance. The peak deflection δ_d = 9.9182 (SC03SD-43.1mm) is highest. The non-dimensional impulse Eqn. (5) & Eqn. (6) are proposed in literature[3]. These equations can be utilised for obtaining the permanent deformation of thin plates.

$$\varnothing_{cs} = \frac{I\left(1+\ln\left(\frac{R_p}{D}\right)\right)}{\left\{\left(1+\ln\left(\frac{S}{D}\right)\right)\pi R_p t^2 (\sigma\rho)^{0.5}\right\}} \quad (5)$$

$$\frac{\delta_p}{t} = 0.427\varnothing_{cs} + 0.298 \quad (6)$$

Figure 5. Experimental test setup and RHA plate perforation after firing.

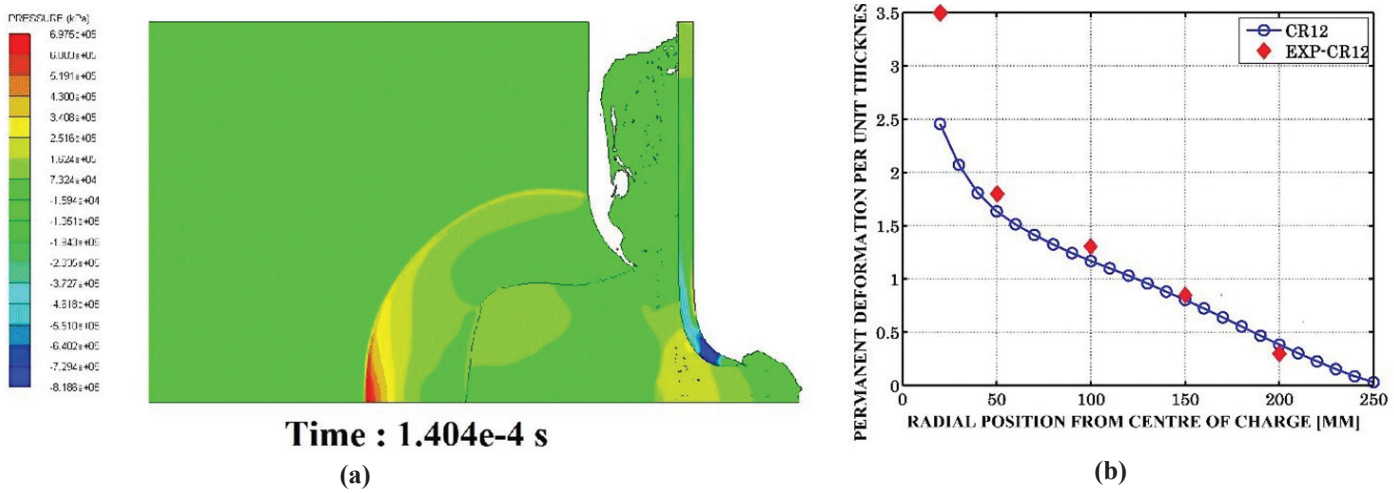

Figure 6. RHA plate deformation in simulation and experiment with CR12 cavity charge.

Using Eqn. (5) and Eqn. (6), the permanent deformation of the plates for different charge shapes have been obtained in Table 5. The permanent deformations for spherical, hemispherical & cylindrical charges are found within the specified variation of 1-2 plate thickness when compared with the simulation results. In addition, the cylindrical charges at a small standoff distance give good results with same equations. Therefore, these equations are applicable in the case of buried charges and the non-dimensional impulse formulation may be utilised for the sand buried charges, if the total impulse is known.

4.3 Influence of Cavity Charges

The failure of the plate is observed in the case of cavity charges. This can be understood from the concept of critical impulse analysis for dishing, discing, and petaling proposed by Lee, *et al.* as given in Eqn. (7)[28]. This equation is based on the uniform rectangular pressure pulse applied to the central region of the circular plate. The uniaxial fracture strain, material flow stress and plate thickness can be utilised for calculating the critical impulse for failure. The critical impulses have been compared with impulses obtained for cavity charges in simulations for plate failure conditions.

$$(I_0)_{cr} = t\sqrt{\frac{32\sigma_0\ \rho\varepsilon_f}{9}} \tag{7}$$

Considering the value of ε_f =0.402 based on JC damage parameters and strain rate with the plastic flow stress value σ_0 = 950 MPa, the critical impulse has been estimated. Since, stress and fracture strain is the strain rate dependent phenomenon, the exact value of σ_0 and ε_f during simulation may vary. The value of the critical impulse is 0.2068 MPa-s. The maximum impulse for C120E, C150E, CR18E, CR15E and CR12E are 0.28387, 0.18738, 0.19167, 0.22949 and 0.33216 respectively. The value of impulse in the case of C150E & CR18 is less than the required quantity of the critical impulse but failure is observed. It is due to the single value of strain and stress taken for the calculation of the critical impulse. In addition, the impulse calculated in the simulation is based on the rigid plate model but in RHA deformation simulations, the deformation of the plate occurs severely under cavity charges as shown in Fig. 6. It cause the change in the flow of the hot gases in the central region and therefore, the pressure duration is longer. This will enhance the impulse density in the central region. The use of the critical impulse can help the designer for estimation of plate thickness, which can survive / fail due to cavity charges.

5. VALIDATION OF FAILURE DUE TO CAVITY CHARGE

Explosive charge of 3.75 kg TNT was considered in the above analysis. The cavity charge of 1.2R created the perforation at a fixed standoff distance in simulation studies. The validation of perforation is carried out in a scale down experiments with the Plastic Explosive (Tetryl 85% and oil 15%). The 137 g of the charge (one third scaled charge) was finalised for the trial based on the scaling technique as used in given reference at one third standoff distance[37]. The plate thickness and radius (t/R_p) ratio of the plate was kept the same.

The simulation was carried out using the earlier methodology for this experimental configuration. The perforation of the plate is shown in Fig. 6(a) due to focused blast pressure. The failure of the RHA plate occurs due to thinning and weakening of the plate at the center due to very high pressure. The deflection of the plate obtained through simulation is shown in Fig. 6 (b) as a CR12 graph. To validate the result in the scale-down experiment, a test setup was developed using the RHA steel plates. The test setup of size 350×390 mm^2 was fabricated using welded armour steel plate. Four holding plates on the frame were welded at four corners. Two RHA plates of 450×400×40 mm^3 having ϕ250 mm cut out were used as holding plates for 10 mm RHA plates by equally spaced eight bolts. The plastic explosive charge is available in the dough form. It was weighed and then using a card sheet cylinder, the cylindrical shape of charge was prepared. This cylindrical charge was pressed with a plastic disc of 1.2R radius to form the hemispherical shape in the front of the charge. The charge of cylindrical charge with 1.2R spherical cavity (L=41.3, D=72.64 mm & Cavity radius of 43.56 mm) was prepaared using this technique. The polystyrene disc at the backside of the charge was used for holding the detonator. The charge was buried in the sand such that it has created a standoff distance of 39.36 mm from the plate as shown in Fig. 5. The RHA plates were further clamped with four bolts to the main test setup after placing the charge in buried condition. An explosive charge was fired using a detonator with the help of a dynamo. After firing, the RHA plate was removed. The deformation and perforation of the plate were measured. Perforated hole and deflection are plotted in Fig. 6(b) as EXP-CR12 against the results obtained through simulation (CR-12). The experimental results validated the perforation of RHA due to the cavity effect of charge.

6. CONCLUSIONS

The detailed study was carried out to assess detonation behaviour of different shapes of explosive charge on failure of RHA plate in near field blast of sand buried charge. The main conclusions drawn from the current study are summarised as follows;

- The highest specific impulse is produced by hemispherical cavity charge of radius R1.2. The permanent and maximum dynamic deformation of buried charges is studied. The Eq. (5) and Eq. (6) can be utilised for predicting the deformation of plate in buried explosive conditions of spherical and cylindrical shapes up to standoff distance more than 0.5D. The failure is attributed to excess amount of specific impulse generated at the centre of the conical / hemispherical cavity charge more than critical impulse.
- If correct specific impulse and its distribution across the charge radius are determined, the failure can be predicted using Eq. (7) with the help of critical impulse equation.
- The damage in scale-down experiments can be validated as suggested for blast experiments for the determination of permanent and dynamic deformation.

REFERENCES

1. Held, M. Anti-tank Mine Blast Effects. *J. Battlef. Technol*., 2009, **12**(1).
2. Zakrisson, B.; Wikman, B. & Häggblad, H-Å. Numerical simulations of blast loads and structural deformation from near-field explosions in air. *Int. J. Impact Eng.,* 2011, **38,** 597–612. doi: 10.1016/j.ijimpeng.2011.02.005.
3. Xiao, W.; Andrae, M. & Gebbeken, N. Air blast TNT equivalence concept for blast-resistant design. *Int. J. Mech. Sci.,* 2020, **185**, 105871. doi: 10.1016/j.ijmecsci.2020.105871.
4. Command USAM, Engineering design handbook Explosions in air, Part one. Army Materiel Command Post; 1974.
5. Knock, C. & Davies, N. Blast waves from cylindrical charges. *Shock Waves,* 2013, **23,** 337–43. doi: 10.1007/s00193-013-0438-7.
6. Knock, C. & Davies, N. Predicting the peak pressure from the curved surface of detonating cylindrical charges. *Propellants Explos. Pyrotech.,* 2011, **36**, 203–9. doi: 10.1002/prep.201000001.
7. Knock, C.; Davies, N. & Reeves, T. Predicting blast waves from the axial direction of a cylindrical charge. *Propellants, Explos Pyrotech.,* 2015, **40**, 169–79. https://doi.org/10.1002/prep.201300188.
8. Wu, C.; Fattori, G.; Whittaker, A. & Oehlers, D.J. Investigation of air-blast effects from spherical and cylindrical-shaped charges. *Int. J. Prot. Struct.,* 2010, **1**, 345–62. doi: 10.1260/2041-4196.1.3.345.
9. Hryciów, Z.; Borkowski; W.; Rybak, P. & Wysocki, J. Influence of the shape of the explosive charge on blast profile. *J. KONES Powertrain Transp.,* 2014, **21**, 169–76. doi: 10.5604/12314005.1130466.
10. Mehreganian, N.; Louca, L.A.; Langdon, G.S.; Curry, R.J. & Abdul Karim, N., The response of mild steel and armour steel plates to localised air-blast loading-comparison of numerical modelling techniques. *Int. J. Impact Eng.,* 2018, **115**, 81–93. doi: 10.1016/j.ijimpeng.2018.01.010.
11. Rajendran, R. & Narasimhan, K. Deformation and fracture behaviour of plate specimens subjected to underwater explosion-a review. *Int. J. Impact Eng.,* 2006, **32**, 1945–63. doi: 10.1016/j.ijimpeng.2005.05.013.
12. Olson, M.D.; Nurick, G.N. & Fagnan, J.R. Deformation and rupture of blast loaded square plates-predictions and experiments. *Int. J. Impact Eng.,* 1993, **13**, 279–91. doi: 10.1016/0734-743X(93)90097-Q.
13. Chung, K.Y.S.; Nurick, G.N.; Verster, W.; Jacob, N.; Vara, A.R.; Balden, V.H.; Bwalyaa, D.; Govendera, R.A. & Pittermanna, M. Deformation of mild steel plates subjected to large-scale explosions. *Int. J. Impact Eng.,* 2008, **35**, 684–703. doi: 10.1016/j.ijimpeng.2008.02.001.
14. Chung, K.Y.S.; Nurick, G.N.; Langdon, G.S. & Iyer, Y. Deformation of thin plates subjected to impulsive load: Part III – an update 25 years on. *Int. J. Impact Eng.,* 2017, **107**, 1339–51. doi: 10.1016/j.ijimpeng.2016.06.010.
15. Zhao, X.; Tiwari, V.; Sutton, M.A.; Deng, X.; Fourney, W.L. & Leiste, U. Deformation scaling of circular plates subjected to dynamic loading. *Procedia IUTAM,* 2012, **4**, 196–205. doi: 10.1016/j.piutam.2012.05.021.
16. Kazemahvazi, S.; Radford, D.; Deshpande, V.S. & Fleck, N.A. Dynamic failure of clamped circular plates subjected to an underwater shock. *J. Mech. Mater. Struct.,* 2007, **2**, 2007–23. doi: 10.2140/jomms.2007.2.2007.
17. Collignon, L.H.A. Influence of the explosion center on shock wave propagation in a confined room. *Shock Waves,* 2020. doi: 10.1007/s00193-020-00946-z.
18. Ambrosini, D.; Luccioni, B.; Nurick, G.; Langdon, G. & Jacob, N. The effect of confinement and stand-off distance in blast tests. *Mecánica Comput.,* 2009, **XXVIII**, 343–62.
19. Peles, S.; Touati, D.; Azulay, I. & Neuberger, A. Numerical simulation of mine detonation beneath a generalized add-on armor structure. Proc - 24th Int. Symp Ballist Ballist., 2008, **1**, 439–47.
20. Heider, N. & Klomfass A. Numerical and experimental analysis of the detonation of sand-buried mine. 22nd Int. Symp. Ballist., 2005, 1389-1396.
21. Hoyos Uribe, J.A.; Bastidas Poveda, V.H. & Casas Rodriguez, J.P. Effect of set up parameters of landmine blast over transferred energy to a rigid body : Experimental and computational study. 26th Int. Symp Ballist., 2011.
22. Clarke, S.D.; Fay, S.D.; Warren, J.A.; Tyas, A.; Rigby, S.E.; Reay, J.J.; Liveseyc, R. & Elgyc, I. Predicting the role of geotechnical parameters on the output from shallowly buried explosives. *Int. J. Impact Eng.,* 2017, **102**, 117–28. doi: 10.1016/j.ijimpeng.2016.12.006.
23. Pickering, E.G.; Chung, K.Y.S. & Nurick, G.N. The influence of the height of burial of buried charges - Some experimental observations. *Int. J. Impact Eng.,* 2013, **58**, 76–83. doi: 10.1016/j.ijimpeng.2013.03.001.
24. Pickering, E.G.; Chung, K.Y.S.; Nurick, G.N. & Haw, P. The response of quadrangular plates to buried charges. *Int. J. Impact Eng.,* 2012, **49**, 103–14. doi: 10.1016/j.ijimpeng.2012.05.007.
25. Zhao, X.; Tiwari, V.; Sutton, M.A.; Deng, X.; Fourney, W.L. & Leiste, U. Scaling of the deformation histories for clamped circular plates subjected to blast loading by buried charges. *Int. J. Impact Eng.,* 2013, **54**, 31–50. doi: 10.1016/j.ijimpeng.2012.10.016.
26. Micallef, K.; Fallah, A.S.; Pope, D.J. & Louca, L.A. The dynamic performance of simply-supported rigid-plastic circular steel plates subjected to localised blast loading. *Int. J. Mech. Sci.,* 2012, **65**, 177–91. doi: 10.1016/j.ijmecsci.2012.10.001.

27. Gharababaei, H.; Darvizeh, A. & Darvizeh, M. Analytical and experimental studies for deformation of circular plates subjected to blast loading, *J. Mech. Sci. Technol.* 2010, **24**, 1855–64. doi: 10.1007/s12206-010-0602-2.
28. Lee, Y.W. & Wierzbicki, T. Fracture prediction of thin plates under localized impulsive loading. Part I: Dishing. *Int. J. Impact Eng.,* 2005, **31**, 1253–76. doi: 10.1016/j.ijimpeng.2004.07.010.
29. Walters, W.P.; William, P. & Zukas, J.A. Fundamentals of shaped charges. John Wiley Sons 1989:398.
30. Choudha, P.K.; Kumaraswamy, A.; Dutta, G.G. & Dhote, K.D. Effect of shape of explosive charge in failure of rolled homogenous armour plate. *Procedia. Struct. Integr.,* 2019, **14,** 191–8. doi: 10.1016/j.prostr.2019.05.025.
31. Chung, K.Y.S.; Langdon, G.S.; Nurick, G.N.; Pickering, E.G. & Balden, V.H. Response of V-shape plates to localised blast load: Experiments and numerical simulation. *Int. J. Impact Eng.,* 2012, **46**, 97–109. doi: 10.1016/j.ijimpeng.2012.02.007.
32. Chapman, T.C.; Rose, T.A. & Smith, P.D., Blastwave simulation using AUTODYN2D: A parametric study. *Int. J. Impact Eng.,* 1995, **16**, 777–87. doi: 10.1016/0734-743X(95)00012-Y.
33. Li, Y.; Wu, W.; Zhu, H.; Wu, Z. & Du, Z. The influence of different pre-formed holes on the dynamic response of square plates under air-blast loading. *Eng. Fail Anal.,* 2017, **78**, 122–33. doi: 10.1016/j.engfailanal.2017.03.002.
34. Bonorchis, D. & Nurick, G.N. The influence of boundary conditions on the loading of rectangular plates subjected to localised blast loading - Importance in numerical simulations. *Int. J. Impact Eng.,* 2009, **36**, 40–52. doi: 10.1016/j.ijimpeng.2008.03.003.
35. Henchie, T.F.; Chung, K.Y.S; Nurick, G.N.; Ranwaha, N.; Balden, V.H. The response of circular plates to repeated uniform blast loads: An experimental and numerical study. *Int. J. Impact Eng.,* 2014,**74**, 36–45. doi: 10.1016/j.ijimpeng.2014.02.021.
36. Nurick, G.N.; Mahoi, S. & Langdon, G.S. The response of plates subjected to loading arising from the detonation of different shapes of plastic explosive. *Int. J. Impact Eng.,* 2016, **89**, 102–13. doi: 10.1016/j.ijimpeng.2015.11.012.
37. Neuberger, A.; Peles, S. & Rittel, D. Scaling the response of circular plates subjected to large and close-range spherical explosions. Part I: Air-blast loading. *Int. J. Impact Eng.,* 2007, **34**, 859–73. doi: 10.1016/j.ijimpeng.2006.04.001.
38. Neuberger, A.; Peles, S. & Rittel, D. Scaling the response of circular plates subjected to large and close-range spherical explosions. Part II: Buried charges. *Int. J. Impact Eng*., 2007, **34**, 874–82. doi: 10.1016/j.ijimpeng.2006.04.002.
39. Banerjee, A.; Dhar, S.; Acharyya, S.; Datta, D. & Nayak, N. Determination of Johnson cook material and failure model constants and numerical modeling of Charpy impact test of armour steel. *Mater. Sci. Eng. A.,* 2015, **640**, 200–9. doi: 10.1016/j.msea.2015.05.073.
40. Mehreganian, N.; Louca, L.A.; Langdon, G.S.; Curry, R.J. & Abdul Karim, N. The response of mild steel and armour steel plates to localised air-blast loading comparison of numerical modelling techniques. *Int. J. Impact Eng.,* 2018, **115**, 81–93. doi: 10.1016/j.ijimpeng.2018.01.010.
41. Liu, M.B.; Liu, G.R.; Lam, K.Y. & Zong, Z. Meshfree particle simulation of the detonation process for high explosives in shaped charge unlined cavity configurations. *Shock Waves,* 2003, **12**, 509–20. doi: 10.1007/s00193-003-0185-2.

ACKNOWLEDGMENTS

The authors are thankful to Sri Haribhau Markale, and Sri VK Dixit, AD, ARDE, Pune for their motivation and support in carrying out the above work. One of the authors Mr Pankaj Choudha is grateful to Vice-Chancellor, DIAT (DU), Pune for allowing him to pursue doctoral work.

CONTRIBUTORS

Mr Pankaj K. Choudha is currently working as Scientist F in DRDO-ARDE. He has obtained his M.Tech (Design) from IIT Bombay. He has contributed significantly in development of Anti-tank and soft target munitions for Indian army.
He has carried out conceptualisation of problem, simulations and experimental studies and writing the draft manuscript as requirements of his PhD work.

Prof. A. Kumarasamy is currently working as Professor, Department of Mechanical Engineering, Defence Institute of Advanced Technology, Pune. His areas of interest are: Solid mechanics, stress analysis, tribology, high strain rate flow behaviour and finite element analysis.
In the present work, he has guided in analysis of critical results and reviewed the manuscript.

Mr V. Venkateswara Rao is currently working as Director, DRDO-ARDE, Pune. He has significantly contributed in AGNI programme.
He has guided and facilitated the team in theoretical and experimental activities and reviewed the manuscript.